The 15th International Symposium on Magnetic Bearings, August 3-6, 2016, Mojiko Hotel, Kitakyushu, Japan

ISMB15

Characteristic Model Based All-Coefficient Adaptive Control of a High-Speed Desorption Pump Supported by AMBs

Long DI*, Chao Yun CHEN**, Chung Hsien LIN** and Zongli LIN*

* Rotating Machinery and Controls (ROMAC) Laboratory and Charles L. Brown Department of Electrical and Computer Engineering, University of Virginia, Charlottesville, VA 22904-4743, USA

ld4vv@virginia.edu, zl5y@virginia.edu

** Industrial Technology Research Institute, Hsinchu, Taiwan 31040, R.O.C.

cychen1022@itri.org.tw, alowlin@itri.org.tw

Abstract

Active magnetic beatings (AMBs) have been increasingly adopted in industries that involve high-speed rotating machinery and feedback control design is one of the essential problems in AMB systems. In this paper, we report on the development of the characteristic model based all-coefficient adaptive control (ACAC) method to a high-speed desorption pump supported by AMBs. This control method does not require the actual system model and is able to deliver strong performance and robustness, as validated in many successful engineering applications. The desorption pump studied in this paper is designed to operate at a speed of 60,000 rpm, which indicates that a potentially large unbalance force might be introduced to drive the AMB system into instability. Meanwhile, the rising speed range is wider than typical machines so that the natural modes can split more significantly due to the gyroscopic effect, which will introduce strong uncertainties. Therefore, a successful controller must guarantee the closed-loop stability and minimize the vibration during the speed increase as well as at the operational speed. The simulation results have demonstrated the proposed ACAC method is capable of achieving the control requirements and the controller will be implemented on the test rig for experimental validations.

Key words : AMB, characteristic model, adaptive control, desorption pump, robustness

1. Introduction

High-speed rotating machineries supported by active magnetic bearings (AMBs) have found more and more applications in the industry (Schweitzer and Maslen, 2009). As the rotating speed increases, the unbalance forces, the gyroscopic effect and the high frequency flexible modes all affect the operation of the machine. Since the controller plays a critical role in the operation of an AMB system, the control design entails significant attention. For a system with complex dynamics, such as a high-speed desorption pump supported by AMBs, a controller with simple structure might not be adequate to achieve the stability and performance requirements. Therefore, advanced controllers are introduced.

Most advanced controllers require system models, which can be difficult to obtain for practical AMB systems. Besides, the design process can be time consuming, especially when large modeling errors are present. The desorption pump analyzed in this paper is designed to operate at a speed of 60,000 rpm, which indicates that a potentially large unbalance force can be introduced to induce instability to the AMB system. Meanwhile, the rising speed range is wider than typical machines so that the gyroscopic effect can split the natural modes more significantly, which will introduce strong uncertainties. Therefore, for our high-speed desorption pump test rig, a successful controller must guarantee the closed-loop stability and minimize the vibration during the speed increase and at the operational speed. In order to satisfy the stringent performance specifications in the face of uncertainties, we adopt the characteristic model based all-coefficient adaptive control (ACAC) method (Wu et al., 2007).

The characteristic model based ACAC method does not require an actual plant model (Wu et al., 2007). It relies on a second order time-varying difference equation that serves as the characteristic model and uses a gradient adaptive algorithm to generate the characteristic parameter estimates, which are then used as the indirect adaptive control parameters. Many successful industrial applications, including aerospace applications, of the characteristic model based ACAC method have been reported (Wu et al., 2007; Zhang and Hu, 2012; Di and Lin, 2014).

In this paper, we apply the characteristic model based ACAC method to a desorption pump supported by AMBs to

improve the system performance and robustness. The paper is organized as follows. First, the test rig is introduced in Section 2. Then we describe the entire AMB system model for simulation study in Section 3. Afterwards, in Sections 4 and 5, the characteristic model based ACAC method are presented and verified by simulations. The concluding remarks are provided in Section 6.

2. The Desorption Pump Test Rig

The desorption pump test rig was built as a research platform at Industrial Technology Research Institute, Hsinchu, Taiwan. The test rig is designed to operate at a nominal speed of 60,000 rpm. The entire system and the rotor are shown in Figs. 1 and 2, respectively.

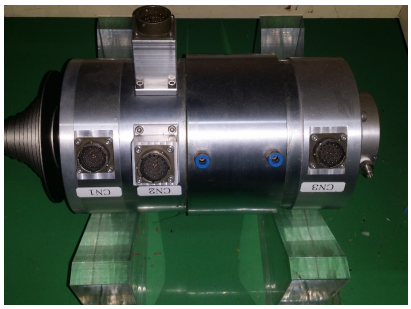

Fig. 1 The desorption pump test rig.

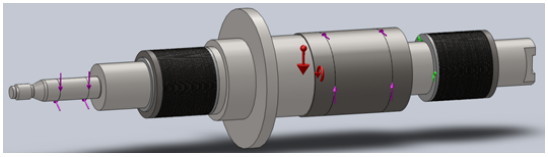

Fig. 2 The rotor diagram.

3. AMB System Model

The AMB system model for the desorption pump equipped with AMBs incorporates the rotor finite element (FE) model, the linearized AMB model, the sensor and amplifier models, and the *Padé* approximation model of the computational delay. The block diagram of the rotor AMB system is shown in Fig. 3.

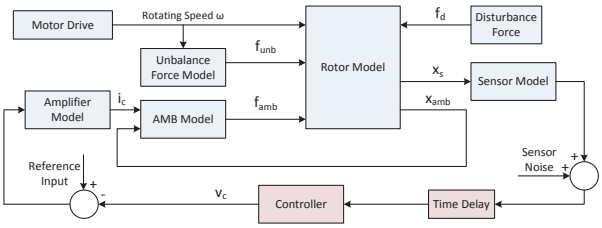

Fig. 3 AMB system block diagram.

3.1. Rotor Model

A two dimensional FE model of the rotor is obtained by dividing the length into 143 stations for the lateral rotor dynamic analysis. The rotor was modeled as a lumped mass-stiffness element while the discs and the AMB laminations are modeled as mass-inertia elements added to certain locations. A four degree of freedom (DOF) lateral analysis is performed for each node. The code generates global entries for the mass (M), internal shaft stiffness (K), internal shaft damping (D) and gyroscopic (G) matrices. Matrices M, K and D are symmetric and positive definite while matrix G is skew-symmetric. The dynamic motion of the rotor can be described in the following second order equation,

$$M\ddot{q} + (D + \Omega G)\dot{q} + Kq = B_{mag}F_{mag} + B_w F_w, \tag{1}$$

$$y_r = Cq, \tag{2}$$

where the displacement vector q contains 572 elements representing the lateral translations in x and y axes, rotating angles about y and x axes, F_{mag} represents the forces provided by the AMBs and B_{mag} specifies the location where the forces are injected, F_w includes all external forces acting on the rotor with B_w specifying the locations, Ω is the rotational speed,

and the vector y_r represents the rotor displacement at the sensor locations specified by the output matrix C. The modeling assumes that there is no axial motion of the rotor.

The critical speed analysis of the rotor as a function of the supporting bearing stiffness is shown Fig. 4. The first five predicted free-free critical speeds are 0 Hz, 0 Hz, 1479.5 Hz, 2740 Hz and 4440 Hz, respectively. The closed-loop stiffness is targeted between 1 MN/m and 10 MN/m. To visualize the gyroscopic effect on splitting the system natural frequencies into forward and backward modes, a Campbell diagram is also generated in Fig. 5. When the running speed lines (1X) and (2X) intersect with the rotor natural frequencies, synchronous or super-synchronous vibrations are induced. These vibrations need to be well-contained with sufficient damping.

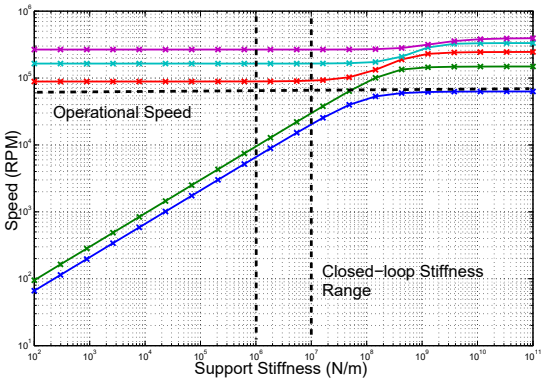

Fig. 4 Critical speed map of the rotor showing the five critical speeds in terms of support stiffness.

The undamped mode shape plot is another important tool to analyze rotordyanmic performance. Since all modes that can be excited should be observable and controllable, the AMBs and sensors should be placed at locations where motions with enough amplitude occur. In addition, the sensor locations need to be in phase with the AMB locations for each natural modes to avoid the non-collocation issue. Shown in Fig. 6 is the undamped mode shape plot of the rotor. It can be observed that non-collocation occurs for the third bending mode. Therefore, an interlacing filter is designed to place suitable zeros between the second and third bending modes and to place suitable poles above the third bending mode.

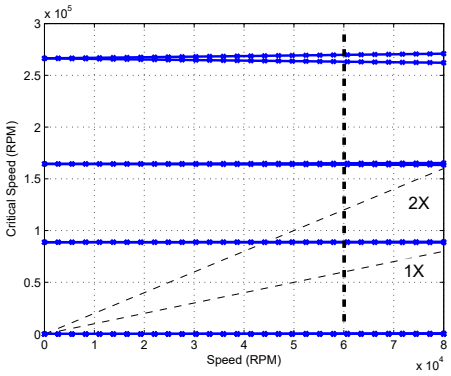

Fig. 5 Campbell diagram of the rotor.

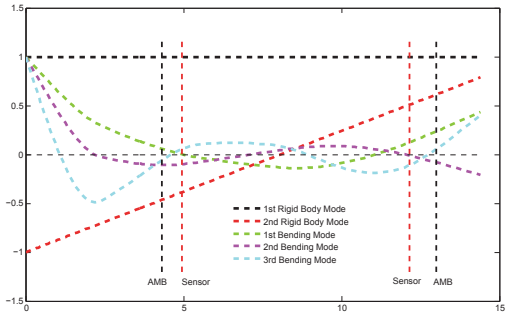

Fig. 6 The undamped mode shape plot of the rotor.

Based on the coordinate transformation between the physical space and the modal space using $q = \Phi_m \zeta$, the state space model based on Eqs. (1) and (2) can be converted into the following modally reduced state space form

$$\begin{bmatrix} \dot{\zeta}_x(t) \\ \dot{\zeta}_y(t) \end{bmatrix} = \begin{bmatrix} A_\zeta & \omega G \\ -\omega G & A_\zeta \end{bmatrix} \begin{bmatrix} \zeta_x(t) \\ \zeta_y(t) \end{bmatrix} + \begin{bmatrix} \Phi_m^{\mathrm{T}} B_{mag} & 0 \\ 0 & \Phi_m^{\mathrm{T}} B_{mag} \end{bmatrix} F_{mag} + \begin{bmatrix} \Phi_m^{\mathrm{T}} B_w & 0 \\ 0 & \Phi_m^{\mathrm{T}} B_w \end{bmatrix} F_w, \tag{3}$$

$$y_r = \begin{bmatrix} C_x \Phi_m & 0 \\ 0 & C_x \Phi_m \end{bmatrix} \begin{bmatrix} \zeta_x(t) \\ \zeta_y(t) \end{bmatrix} \tag{4}$$

The original state space model has 1144 states and contains several high order rotor modes beyond the controller bandwidth. These modes are unlikely to be excited and contribute negligible effect to the system dynamics. Thus, in order to facilitate designs and analysis, model truncation is usually applied to obtain reduced order model. The final rotor model

retains the two rigid body modes and the first three bending modes with a total of 20 states and is represented as follows,

$$\dot{x}_m = A_m x_m + B_m F_{mag} + B_d F_w,$$
$$y_r = C_m x_m.$$

3.2. Modeling of AMBs

The forces generated by AMBs depend on the air gap between the rotor and the stator, as well as the current feedings in the windings on the stator. According to Fig. 7, the following nonlinear equation is derived to describe the net force generated by a pair of electromagnets based on the movement x and the air gap g_0

$$f = f_1 - f_2 = \frac{\mu_0 N^2 A_g I_1^2}{4(g_0 - x)^2} - \frac{\mu_0 N^2 A_g I_2^2}{4(g_0 + x)^2} = \frac{\mu_0 N^2 A_g}{4}\left[\frac{I_1^2}{(g_0 - x)^2} - \frac{I_2^2}{(g_0 + x)^2}\right]. \tag{5}$$

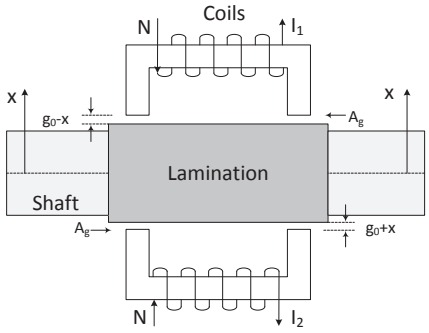

Fig. 7 AMB operating principle.

With I_1 and I_2 being the bias current I_b perturbed by the perturbation current i as $I_b + i$ and $I_b - i$, respectively, linearization of f around the equilibrium point ($i = 0$ and $x = 0$) results in

$$f = \frac{\mu_0 N^2 A_g}{g_0^4}(I_b^2 g_0 x + I_b i g_0^2) = \frac{\mu_0 N^2 A_g I_b^2}{g_0^3} x + \frac{\mu_0 N^2 A_g I_b}{g_0^2} i, \tag{6}$$
$$f = k_x x + k_i i, \tag{7}$$

where $k_x = \frac{\mu_0 N^2 A_g I_b^2}{g_0^3}$ and $k_i = \frac{\mu_0 N^2 A_g I_b}{g_0^2}$ are the stiffness and current gains, respectively.

This AMB model ignores the eddy current loss and assumes zero leakage in the magnetic circuit. Combining the rotor model with the linearized AMB model, we arrive at the following system model

$$\dot{x}_m = \Big(A_m - B_m k_x [B_{mag} \quad 0]\Big) x_m + B_m k_i i + B_d F_w,$$
$$:= \hat{A}_m x_m + B_m k_i i + B_d F_w,$$
$$y_r = C_m x_m.$$

3.3. The Entire AMB System

Based on the fitting with the experimental frequency response, the power amplifier is modeled by a first order transfer function as follows,

$$G_a(s) = \frac{\text{DC gain}}{(s + p_a)} \text{ A/V}, \tag{8}$$

where the DC gain is 19.39 A/V, $p_a = 21240$, which gives a bandwidth of 2.74 KHz. The amplifier transfer function $G_a(s)$ is then converted into a state space model (A_a, B_a, C_a) with a total of 4 states for all the control channels.

The eddy current type displacement sensor is modeled by the following transfer function

$$G_s(s) = \frac{\text{constant gain}}{(s^2 + 2\xi_1\omega_1 s + \omega_1^2)(s^2 + 2\xi_2\omega_2 s + \omega_2^2)}, \tag{9}$$

where the constant gain is 1.388×10^{22}, $\xi_1 = 0.159$, $\xi_2 = 0.695$, $\omega_1 = 8.6296 \times 10^5 \text{rad}/s$, $\omega_2 = 1.3659 \times 10^5 \text{rad}/s$. The sensor transfer function $G_s(s)$ is converted into a state space model (A_s, B_s, C_s) with 16 states.

To model the computational delay caused by the DSP, a second order *Padé* approximation is used to obtain a rational transfer function for a approximated time delay as follows

$$e^{-\tau s} = \frac{e^{-\frac{1}{2}\tau s}}{e^{\frac{1}{2}\tau s}} \approx \frac{1 - \frac{1}{2}\tau s + \left(\frac{1}{2}\tau s\right)^2}{1 + \frac{1}{2}\tau s + \left(\frac{1}{2}\tau s\right)^2}. \tag{10}$$

The *Padé* approximation can be formulated into a state space model (A_f, B_f, C_f) that contributes 8 additional states. The final system model incorporating the rotor, AMBs, amplifiers, sensors and time delay can be described in the following form,

$$\begin{bmatrix} \dot{x}_m \\ \dot{x}_s \\ \dot{x}_a \\ \dot{x}_f \end{bmatrix} = \begin{bmatrix} \hat{A}_m & 0 & B_m k_i C_a & 0 \\ B_s C_m & A_s & 0 & 0 \\ 0 & 0 & A_a & 0 \\ 0 & B_f C_s & 0 & A_f \end{bmatrix} \begin{bmatrix} x_m \\ x_s \\ x_a \\ x_f \end{bmatrix} + \begin{bmatrix} 0 \\ 0 \\ B_a \\ 0 \end{bmatrix} u + \begin{bmatrix} B_d \\ 0 \\ 0 \\ 0 \end{bmatrix} F_w, \tag{11}$$

$$y_f = C_f x_f. \tag{12}$$

4. Characteristic Model Based All-Coefficient Adaptive Control

4.1. Characteristic Modeling

While conventional modeling methods focus on the precise system dynamics, the characteristic modeling concentrates on the characteristics of the plant and the control performance requirements. The corresponding output information of the original high order plant is compressed into several characteristic parameters so that no information is lost during the modeling process (Wu et al., 2007). As a result, the characteristic model closely reflects the dynamics of the original plant while it possesses a simple structure.

Consider the following linear time-invariant plant

$$G(s) = \frac{b_m s^m + b_{m-1} s^{m-1} + \cdots + b_1 s + b_0}{s^n + a_{n-1} s^{n-1} + \cdots + a_1 s + a_0}. \tag{13}$$

It can be represented by a time-varying difference equation with a lower order and the exact order is related to the control objective.

For a linear time-invariant plant as given in (13), if the control objective is position keeping or constant reference tracking, then, for a sufficiently small sampling period T that satisfies the sampling theorem, the characteristic model can be represented by a second-order time-varying difference equation (Wu et al., 2008),

$$y(k) = f_1(k-1)y(k-1) + f_2(k-1)y(k-2) + g_0(k-1)u(k-1) + g_1(k-1)u(k-2), \tag{14}$$

where $u(k)$ and $y(k)$ are respectively the control input and the system output and the coefficients $f_1(k)$, $f_2(k)$, $g_0(k)$ and $g_1(k)$ are the characteristic parameters.

The characteristic model (14) possesses the following properties:

- Coefficients $f_1(k)$, $f_2(k)$, $g_0(k)$ and $g_1(k)$ are slowly time varying.
- The ranges of the characteristic parameters can be decided *a priori*.

4.2. Characteristic Model Based All-coefficient Adaptive Control

Consider a linear time-invariant plant

$$y^{(n)} = a_{n-1} y^{(n-1)} + \cdots + a_0 y + b_m u^{(m)} + \cdots + b_0 u. \tag{15}$$

The discretized equation of (15) can be described as follows,

$$y(k+n) = \alpha_1 y(k+n-1) + \cdots + \alpha_n y(k) + \beta_0 u(k+m) + \cdots + \beta_m u(k). \tag{16}$$

Then, the coefficients of (16) satisfy the following conditions

- If the static gain D of (15) is equals to unity, then the sum of all the coefficients of (16) equals one, *i.e.*, $\sum_{i=1}^{n} \alpha_i + \sum_{i=0}^{m} \beta_i = 1$.
- If $D \neq 0$ and is bounded, then the sum of all the coefficients of (16) approaches one as $T \to 0$, *i.e.*, $\lim_{T \to 0} \left(\sum_{i=1}^{n} \alpha_i + \sum_{i=0}^{m} \beta_i \right) = 1$.

The ranges of α_i's and β_i's can be determined in advance based on the ranges of a_i's and b_i's. The value of the sampling period T, when system (15) does not have poles at the origin, is usually chosen as

$$T \in \left[\frac{T_{\min}}{15}, \frac{T_{\min}}{3}\right],$$

where $T_{\min}$ is the minimum average time constant of system (15) over the ranges of the values of its coefficients a_i's and b_i's. The value of $T_{\min}$ can be determined in a straightforward way as follows.

Let C denote the set of values of the coefficients a_i's and b_i's. Clearly, the poles of system (15), denoted as p_i, $i = 1, 2, \cdots, n$, are functions of the elements of C. Then, the minimum average time constant $T_{\min}$ can be computed as

$$T_{\min} = \min_{C} \frac{1}{\left(\prod_{i=1}^{n} |p_i|\right)^{\frac{1}{n}}} = \frac{1}{\left(\max_{C} |a_0|\right)^{\frac{1}{n}}}.$$

We now consider the characteristic model (14) and rewrite it as follows to facilitate the coefficient estimations,

$$y(k) = \phi^T(k-1)\theta(k-1),$$

with

$$\phi(k-1) = [y(k-1) \quad y(k-2) \quad u(k-1) \quad u(k-2)]^T,$$
$$\theta(k-1) = [f_1(k-1) \quad f_2(k-1) \quad g_0(k-1) \quad g_1(k-1)]^T.$$

In order to specify the ranges of the values of the coefficients in the characteristic model (14), we first consider the following second order time-invariant difference equation

$$y(k) = \alpha_1 y(k-1) + \alpha_2 y(k-2) + \beta_0 u(k-1) + \beta_1 u(k-2). \tag{17}$$

Let

$$\eta_{\max} = \frac{T}{T_{\min}},$$

and according to (Wu et al., 2008), when $\eta_{\max} \leq \frac{1}{3}$, the coefficients in the characteristic model (14) for an unstable plant satisfy the following conditions:

$$\begin{cases} 2\cos(\frac{\eta_{\max}}{2}) \leq \alpha_1 \leq 2e^{\frac{\eta_{\max}}{2}}, \\ -e^{\eta_{\max}} < \alpha_2 \leq -1, \\ 2e^{\frac{\eta_{\max}}{2}} \cos\left(\frac{\eta_{\max}}{2}\right) - e^{\eta_{\max}} \leq \alpha_1 + \alpha_2 \leq 1, \\ \frac{b_0 T^2}{2} < \beta_0 < \frac{b_0 T^2}{2}\left(1 + \frac{\eta_{\max}}{3} + \frac{\eta_{\max}^2}{12}\right), \\ \frac{b_0 T^2}{2}\left(1 - \frac{\eta_{\max}^2}{24}\right) < \beta_1 < \frac{b_0 T^2}{2}\left(1 + \frac{2\eta_{\max}}{3} + \frac{7\eta_{\max}^2}{24}\right). \end{cases}$$

Given the conditions above, it can be observed that $\alpha_1 \to 2$, $\alpha_2 \to -1$, $\beta_0 \to 0$ and $\beta_1 \to 0$, as $T \to 0$ and (hence $\eta_{\max} \to 0$). For a particular value of $\eta_{\max} = \frac{1}{4}$, we arrive at the following ranges for the coefficients α_1 and α_2,

$$\begin{cases} \alpha_1 \in [1.9844, 2.2663], \\ \alpha_2 \in [-1.2840, -1], \\ \alpha_1 + \alpha_2 \in [0.9646, 1]. \end{cases}$$

On the other hand, β_0 and β_1 are smaller positive scalars.

Motivated by the above analysis on the second order time invariant difference equation (17), we will limit the coefficients $f_1(k)$ and $f_2(k)$ in the characteristic model (14) to the following set

$$\mathcal{N} = \{(f_1, f_2) : 1.9844 < f_1 < 2.2663, \ -1.2840 < f_2 < -1\},$$

and choose some positive numbers that are much smaller than one as the initial values for $g_0(k)$ and $g_1(k)$.

Let $\phi^T(k)$ represent the input and output variables, $\hat{\theta}(k) = [\hat{f}_1(k) \quad \hat{f}_2(k) \quad \hat{g}_0(k) \quad \hat{g}_1(k)]^T$ be the estimate of vector $\theta(k)$ which contains the coefficients of the characteristic model. Then, the estimation error $\epsilon(k)$ is given as

$$\epsilon(k) = y(k) - \phi^T(k-1)\hat{\theta}(k-1).$$

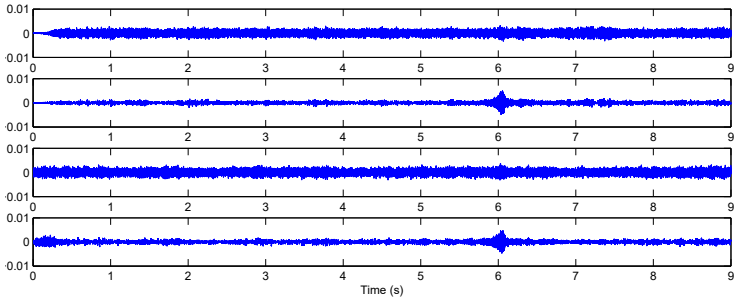

Fig. 8 The rotor displacements of the four radial axes as the speed increases linearly with time from 0 to 60,000 rpm.

The estimate $\hat{\theta}(k)$ can be updated by the gradient adaptive law along with a parameter projection as follows,

$$\hat{\theta}_u(k) = \hat{\theta}(k-1) + \frac{\gamma\phi(k-1)\epsilon(k)}{\delta + \phi^T(k-1)\phi(k-1)},$$
$$\hat{\theta}(k) \ = \pi\left(\hat{\theta}_u(k)\right),$$

where $\delta \geq 0$, $0 < \gamma < 2$, $\pi(x)$ is the projection of x into the given bounded set $\mathcal{N}$.

The characteristic model based ACAC output $u_c(k)$ in this research is formulated as,

$$u_c(k) = u_{c1}(k) + u_{c2}(k) + u_{c3}(k),$$

where

- Maintaining/tracking control law
$$u_{c1}(k) = \frac{y_{\mathrm{r}}(k) - \hat{f}_1(k)y(k) - \hat{f}_2(k)y(k-1) - \hat{g}_1(k)u_{c1}(k-1)}{\hat{g}_0(k) + \lambda_1},$$

where $y_{\mathrm{r}}(k)$ is the reference system output and λ_1 is a positive constant.

- Golden section adaptive control law
$$u_{c2}(k) = \frac{l_{c1}\hat{f}_1(k)\tilde{y}(k) + l_{c2}\hat{f}_2(k)\tilde{y}(k-1) + \hat{g}_1(k)u_{c2}(k-1)}{\hat{g}_0(k) + \lambda_1},$$

where $\tilde{y}(k) = y_{\mathrm{r}}(k) - y(k)$, $l_{c1} = 0.382$ and $l_{c2} = 0.618$ according to the golden section rule.

- Differential control law
$$u_{c3}(k) = d_1\frac{\tilde{y}(k) - \tilde{y}(k-1)}{T},$$

where d_1 is a positive constant.

5. Simulation Results

To verify the proposed characteristic model based ACAC method, we carry out numerical simulation on the AMB system model derived from the actual desorption pump test rig as shown in Eqs. (11) and (12). The simulation program is constructed in Matlab Simulink and the main modeling block for the AMB system is formulated through the Matlab S-function, which makes the interface more compact and the program more flexible for different test rigs. There are four control channels for the x and y axes of both support AMBs. Each channel is controlled by the proposed characteristic model based ACAC controller individually, where all the controllers adopt the same control parameters and initial values for the adaptive law. The control parameters are chosen as $\gamma = 1.5$, $\delta = 0.1$, $\lambda_1 = 2$ and $d_1 = 0.0002$, while the initial conditions of the adaptation law are selected as $f_1(0) = 2.212$, $f_2(0) = -1.052$, $g_0(0) = g_1(0) = 0.01$. Note that $(f_1(0), f_2(0)) \in N$.

Shown in Fig. 8 are the rotor displacements of the four radial axes from 0 to 60,000 rpm. The small vibrations over a wide range of speeds demonstrate the effectiveness and the potential of the proposed control design method.

Shown in Fig. 9 are the rotor displacements of the four radial axes at 60,000 rpm, which is the designed operational speed for the desorption pump. It can be observed that the vibration is well contained and is much smaller than the radial clearance. Fig. 10 shows the corresponding FFT of the vibration signal at 60,000 rpm (1000 Hz), which verifies that no other natural modes have been excited.

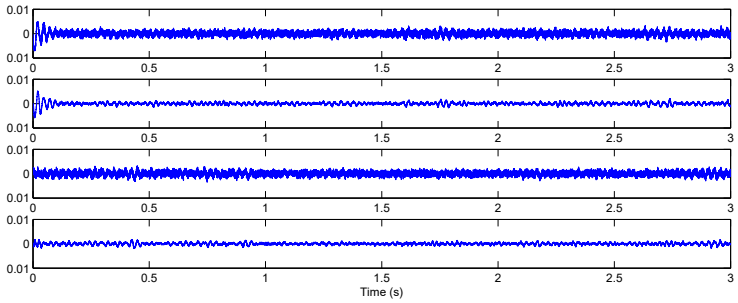

Fig. 9 The rotor displacements of the four radial axes at 60,000 rpm.

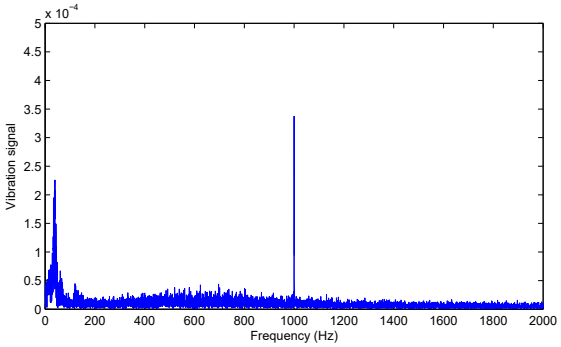

Fig. 10 The FFT of the rotor vibration signal at 60,000 rpm (1000 Hz).

6. Conclusions

This paper investigated the application of the characteristic model based ACAC design to a high speed desorption pump supported by AMBs. The main challenge lies on the high operational speed, which might introduce large disturbance force to the system for small residue unbalance weight. In addition, due to the wide rising speed range, the gyroscopic effect can also drive the natural mode to split more dramatically. These stabilization and robustness problems have been well addressed by the proposed method, as verified by the simulation results.

References

Schweitzer, G. and Maslen, E. H., Magnetic Bearings. Berlin: Springer-Verlag, 2009.

Wu, H. X., Hu, J. and Xie, Y. C., Characteristic Model-based All-coefficient Adaptive Control Method and its Applications, *IEEE Trans. Systems, Man, and Cybernetics, Part C: Applications and Reviews*, Volume 37, Issue 2, page 213-221, 2007.

Zhang, Z. and Hu, J., Stability Analysis of a Hypersonic Vehicle Controlled by the Characteristic Model based Adaptive Controller , *Science in China Series F: Information Sciences*, Volume 55, Issue 10, page 2243-2256, 2012.

Di, L. and Lin, L., Control of a Flexible Rotor Active Magnetic Bearing Test Rig: A Characteristic Model Based All-Coefficient Adaptive Control Approach, *Control Theory and Technology*, Volume 12, Issue 1, page 1-12, 2014.

Wu, H. X., Hu, J. and Xie, Y. C., Characteristic Model-Based Intelligent Adaptive Control. Beijing: China Science and Technology Press, 2008.